CO-REGISTRATION OF TOTAL INTERNAL REFLECTION FLUORESCENCE AND CONFOCAL MICROSCOPY IMAGES FOR STUDYING VESICLE TRAFFICKING IN LIVING CELLS

William T. E. Pitkeathly[†] *Joshua Z. Rappoport*[‡] *Ela Claridge* [⋆]

[†] Physical Sciences of Imaging in the Biomedical Sciences (PSIBS) doctoral training centre, University of Birmingham, Birmingham, B15 2TT, UK.
[‡] School of Biosciences, University of Birmingham, Birmingham, B15 2TT, UK.
[⋆] School of Computer Science, University of Birmingham,Birmingham, B15 2TT, UK.

ABSTRACT

The dynamics of vesicle trafficking via the cell membrane and the tracking of their subsequent movements within the cell are of great interest in the biomedical sciences. One challenge of image analysis is following the vesicle's fate continuously from its formation at the membrane to its final destination, as it requires different microscopy techniques to image the complete journey. Total internal reflection fluorescence (TIRF) microscopy is used for imaging events at the cell membrane and laser scanning confocal microscopy (LSCM) is used for imaging the interior of the cell. We present a simple and robust method for co-registration of data sets from the two microscopy techniques. This method is validated on images generated by computer simulation of the image formation process in TIRF and in LSCM. The registration parameters are recovered with error less than 1% in presence of Gaussian noise up to SNR of 3.8dB. Registration of real microscopy data is shown and the accuracy of the retrieved parameters is compared and agrees well with values obtained manually and a difference in squares measure.

***Index Terms*—** TIRF, confocal, registration, multi-modality, fluorescence microscopy

1. INTRODUCTION

Many intracellular processes can only be studied through direct observation *in situ* via fluorescence microscopy. One such important area is endocytic vesicle trafficking and cargo recycling which studies the transport of molecules into and out of a cell as well as between locations within the cell. Vesicles are small "sacks" formed from lipid membranes which enclose various molecules. In endocytosis extracellular molecules are encapsulated within small vesicles (typically $20 - 100nm$ diameter) formed at the cell membrane through a complex chain of molecular events. Once a vesicle has formed and separated from the membrane, it diffuses away, until it is transported directly to various locations within the cell via microtubules. Depending on the vesicles content, the internalised molecules can be degraded and/or be returned back into the cell membrane, or expelled completely from the cell.

The dynamics of vesicle trafficking via the cell membrane and the tracking of their subsequent movements within the cell are of great interest in the biomedical sciences. The vesicles and their potential target destinations are tagged with fluorescent markers and thus their movement can be studied using fluorescent microscopy. Whereas there exist methods for vesicle tracking close to the cell membrane [1] and throughout cell body[2], one of the challenges that remains is following of the vesicle's fate continuously from its formation at the membrane to its final destination. This is problematic because the ideal light conditions required for imaging the cell membrane at high resolution are different to those for imaging the interior of the cell and therefore require different imaging techniques.

For imaging cell molecular events at the cell membrane total internal reflection fluorescence (TIRF) microscopy is the method of choice [3] since it exclusively illuminates a thin slice of a sample within $\sim 100nm$ of the imaging surface (usually a glass cover slip). If the cell sample is in contact with the imaging surface, and the relevant molecules are tagged with fluorescent markers, then cell membrane events such as vesicle formation can be imaged[4]. The limitation of TIRF is that it cannot image slices deeper than a few hundred nano-meters from the imaging surface, and hence it is inherently 2D. For imaging of the cell interiors laser scanning confocal microscopy (LSCM) is commonly used. It provides a means for of optically sectioning a sample so that sub cellular components, such as vesicles, can be resolved in three dimensions (3D) rather than just two (2D). 3D images are formed of a series of 2D cross-sectional images. Each image slice represents a planar volume $\simeq 1\mu m$ thick (approximately 10 times thicker than TIRF), and thus images usually contain higher levels of background fluorescence compared to TIRF.

This paper presents a method for co-registration of images from total internal reflection fluorescence microscope and laser scanning confocal microscope. It thus bridges an important gap that exist in vesicle tracking. The paper first briefly describes the principles of TIRF and LSCM. The registration algorithm is described next. Validation of the registration technique is carried out using phantom data generated by using the model of image formation in TIRF and in LSCM. Results from the imaging experiments are presented next. The paper concludes with outlining the future perspectives of the vesicle trafficking studies that will be made possible through this work.

2. IMAGE FORMATION

2.1. TIRF microscopy

Total internal reflection fluorescence (TIRF) microscopy exploits the physical properties of an evanescent field to exclusively illuminate a thin section of a sample within a close distance to ($\sim 100nm$) the field's surface of origin. An evanescent field is produced on the reverse side of a boundary of two regions with different refractive indexes when a beam of light is totally internally reflected at this boundary. The field direction of propagation is parallel to the bound-

ary of reflection and its intensity decays with perpendicular distance from it:

$$I_z = I_0 exp(-z/d) \quad (1)$$

where z is the distance from the boundary and d is the decay constant. d is predominantly dependent on wavelength, λ_0, and angle of incidence, θ: $d = \frac{\lambda_0}{4\pi}\left({n_2}^2 sin^2\theta - {n_1}^2\right)^{-1/2}$. Limited illumination depth is beneficial as is causes minimal background fluorescence, and thus, TIRF provides a means for high contrast molecular bio imaging with high auxiliary (z-direction) resolution[4]. TIRF is ideal for imaging molecular events at plasma membrane of cells adhered to the glass coverslip. Images are recorded using a scientific grade CCD camera.

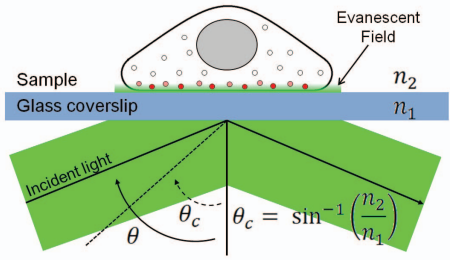


Fig. 1. An illustration of the physical principles of TIRF illumination.

2.2. Laser Scanning Confocal Microscopy

Confocal microscopes use focused point scanning lasers to illuminate a sample, and a photon multiplier tube (PMT) to measure any fluorescence. Photons detected by the PMT have passed through a system of filters and then a small pinhole which the filtered light is focused onto. The purpose of the pinhole is to reject light from out of focus planes, and thus the only photons detected are those confined to a small volume centred at the focal point of the objective lens. This permits what is known as 'optical sectioning' of a sample. Images are formed through scanning line raster operations of the focused laser across a 2D plane through a sample. Acquisition of adjacent parallel 2D planes allows the generation of 3D volumetric images. This capability is the main advantages of confocal microscopy over other techniques.

2.3. TIRF and LSCM combined

Multimodality microscopes exist whereby numerous microscopy techniques, such as TIRF and LSCM, are built onto one module and share a common objective lens. Sequential or simultaneous image acquisition via multiple techniques combines the benefit of each technique and maximises the information available from a single study. For imaging with both TIRF and LSCM, sequential acquisition is performed by mechanically switching their light paths to and from the objective lens. The sequence starts first with an image acquired with TIRF (or several at high frame rate) shortly followed by a 3D volumetric LSCM image, this is then repeated as rapidly as possible (switching from one to the other takes $\sim 1second$). The first slice of the 3D LSCM image should be from the same focal plane as the TIRF image. Because of the difference in image formation processes for each technique and the use of different detection devices, the resulting images are not spatially coincident. In order to correctly track the vesicles imaged using TIRF and LSCM it is necessary to accurately co-register the respective data sets.

3. CO-REGISTRATION

As described above, the two microscopes each have their own characteristics and thus images of the same object often appear significantly different even at the same focal plane. Images from LSCM represent a physically thicker section of a sample than TIRF, features in the LSCM images often appear to be superimposed onto an uneven lower-intensity background and accompanied by other fluorescent structures which are situated beyond the reach of the TIRF illumination field. Even within in the TIRF field, if two identical fluorescent objects lie adjacent in the x-y plane but their position differ slightly (tens of nm) in the z-plane then there intensities will differ whereas they might not in the LSCM image. In addition to these inherent differences, image features are related by three geometrical transformations: scale, rotation, translation. These arise through the use of different optical detection devices (PMT for LSCM, and a CCD for TIRF). The rotation is due to the misalignment of these devices, which are generally fixed in position, and hence, the relative image orientation remains constant. In contrast, each detection device can be configured differently depending on the imaging conditions/type of experiment, and hence, scaling and feature position within an image can change between experiments. The fact that the rotation is constant for a given microscope was exploited to reduce the complexity of the registration algorithm. The rotation parameter is calculated separately once and used subsequently as a pre-registration correction factor. Registration of the individual data sets needs then to consider only scaling and translation.

3.1. Determination of rotational offset

Features common in a given pair of images from the 2 microscopes differ in both rotation and scale. To determine the rotation accurately we require precise knowledge of the image pixel scales. Because of the differences in the relative intensity of features and background structures between the images, registration parameters were calculated in frequency domain rather than using intensity based techniques. An iterative algorithm was developed to optimize for both the angle of rotation and the scale for a TIRF and LSCM image of the same object to maximise the accuracy of the angle of rotation. Phase correlation is used as a similarity metric here. Phase correlation of two images, I_1, and I_2, is defined by:

$$c = \mathcal{F}^{-1}\left\{\frac{\mathcal{F}\{I_1\}\mathcal{F}^*\{I_2\}}{|\mathcal{F}\{I_1\}\mathcal{F}^*\{I_2\}|}\right\} \quad (2)$$

Where: c is equal to the inverse Fourier transform, $\mathcal{F}^{-1}\{\cdot\}$, of the normalised cross-power spectrum between the Fourier transform of first image, $\mathcal{F}\{I_1\}$, and complex conjugate of the Fourier transform the second $\mathcal{F}^*\{I_2\}$. Thus the similarity metric used is:

$$C = \arg\max_{(x,y)}\{c\} \quad (3)$$

The initial estimates for the image scale difference are calculated from the physical resolution of each image which is obtained experimentally. In two parallel 'tests', a scaled-rotated TIRF image, $I_{TIRF}(x, y; s; \theta)$ is compared to an unaltered LSCM image $I_{LSCM}(x, y)$ using the phase correlation metric; one 'test' is for optimisation of the scale, the other for rotation. The parameter being optimised is varied over a range of values, centred at a current estimate, while the other is kept fixed. The optimal value from each test updates the previous estimate and is used as the constant the next test iteration. If S_C, and, S_T, are values for the calibrated pixel resolution for LSCM and TIRF microscope images respectively, then

the ratio gives a relative scale estimate s_{est}. To constrain the search angle, an estimate of the limiting angle θ_{est} is provided. Estimation errors, σ_s and σ_θ are assigned as a range to search over. The full algorithm can be found in the supplementary section of [5].

3.2. Complete registration - Translation and scale

To determine the difference in translation between the features in the TIRF and LSCM images, an algorithm using a combination of normalised cross-correlation (NCC) and an iterative scale correlation test was implemented. The feature scale difference was calculated in the frequency domain using an iterative scale test through comparison of a scaled $I_{TIRF}(x, y; s)$ with an unaltered LSCM image, $I_{LSCM}(x, y)$, over a range of scales. Prior to registration one of the images is rotated by the misalignment angle calculated by the previous algorithm. Briefly: a phase correlation test was performed on down-scaled images using as an initial scale estimate. A NCC algorithm[6] was then used to estimate the translation between the down scaled images scaled by the optimal result from the scale test. This process is then repeated on images at full resolution using only image data from regions that specially overlapped when scaled and translated by the estimates from the previous step. The original full resolution images are then scaled and translated accordingly to achieve registration. Details for the full algorithm are given in [5].

4. MICROSCOPY IMAGE FORMATION SIMULATIONS

To validate the registration process phantom data sets were generated through the simulation of the image formation processes for both TIRF and LSCM microscopes. We can define the image formation process mathematically as:

$$i(x, y; z_0) = N\left(f \otimes h\right)(x, y, z) \tag{4}$$

Where: $i(x, y; z_0)$ is the image, from the focal point z_0 of the objective, $\otimes$ denotes the convolution between the 3D fluorophore distribution, $f(x, y, z)$, and the point spread function $h(x, y, z)$ of our optical system, and $N(\cdot)$ is a noise process function. Both photon (Poisson), and readout (Gaussian) noise processes occur in fluorescent microscopy detection systems. Here, for simplicity, we approximate noise as an additive Gaussian process, thus Equation (4) becomes:

$$i(x, y; z_0) = \left(f \otimes h + n\right)(x, y, z) \tag{5}$$

Where $n(x, y, z)$ is a Gaussian noise function. In light microscopy, the point spread function describes the interference pattern (or observation volume), $psf_{OBJ}(x, y, z)$, in the back focal plane of the objective lens due to light falling on its spherical aperture from a point source the at the front focal plane. For LSCM, this function not only describes the observation volume, $psf_{obs}(x, y, z)$, but also the illumination volume, $psf_{ill}(x, y, z)$, of the focused laser light in the front focal plane [7]. Therefore the effective point spread function for LSCM is the product of these: $h_{LSCM} = psf_{obs}(x, y, z) \cdot psf_{ill}(x, y, z) = psf^2_{OBJ}(x, y, z)$. From this we get our LSCM image:

$$i_{conf}(x, y; z_0) = \left(f \otimes (psf^2_{OBJ}) + n\right)(x, y, z) \tag{6}$$

For TIRF the 3D illumination intensity function, $l(x, y, z)$, can be approximated as being spatially invariant in the x-y plane (a Gaussian laser beam profile can cause intensity drop off at edges) but decreases exponentially with distance the imaging surface in the z direction according to Equation (1). The fluorophore distribution function is then profiled by this intensity distribution prior to the convolution with the point spread function of the objective, $psf_{OBJ}(x, y, z)$. The expression for the TIRF image becomes:

$$i_{TIRF}(x, y; z_0) = ((f \cdot l) \otimes psf_{OBJ} + n)(x, y, z) \tag{7}$$

The point spread function for $psf_{OBJ}(x, y, z)$ used here was taken from Appendix. A. in [7]. The expression given was solved numerically using MATLAB's *trapz()* function for an objective lens with a numerical aperture of 1.49, immersion oil refractive index of 1.51 with each pixel representing $100nm$ in each dimension. A phantom object was defined in 3D space then subjected to the image simulation processes above. The object consisted of numerous sub-diffraction points or lines randomly distributed within a 3D ellipsoid imitating biological structures such as vesicles or microtubules. Before noise was added, the LSCM image was scaled and the TIRF image was rotated and translated by some known amount to mimic the difference in acquisition devices. Different levels of Gaussian noise were added and images were grouped into 3 noise categories: *Hi-SNR* $\approx 16dB$, *Med-SNR* $\approx 7dB$, and, *Low-SNR* $\approx 4dB$.

5. RESULTS

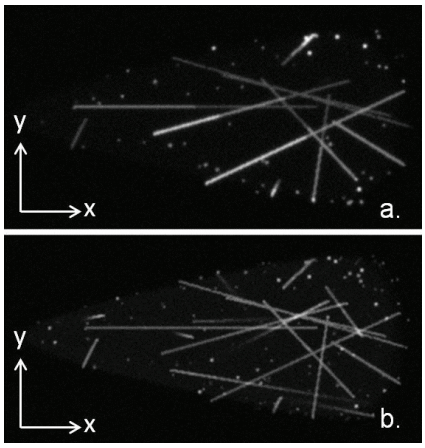


Fig. 2. Images of a phantom generated using the mathematical image formation simulations of a. TIRF and b. LSCM.

Five phantom images pairs were generated using the image formation processes described above. The TIRF image was simulated to have a $150\mu m$ penetration depth and the LSCM volume was $1\mu m$ using excitation wavelength of $488nm$. The feature in the TIRF image was translated by 20 pixels exactly in both x and y directions. The LSCM images were then scaled by a factor of 0.95, and the TIRF images rotated by 4^o anti-clockwise. Images were then distorted with 3 levels of additive Gaussian noise to produce 3 groups of 5 image pairs. Robustness of algorithms were tested using these data sets. Figure 2 is an example of the phantom images(cropped). There are features in visible the LSCM image (fig. 2 b.) that are not in the TIRF (fig. 2 a.), this is because the simulated 'slice' thickness of the LSCM is greater than that in the TIRF. The intensity of the line structures in the TIRF image varies along their length with respect to the z-distance to the illumination field (as expected according to Equation (1)).

5.1. Rotation

The algorithm for calculating the rotational displacement due to the detection hardware offset was tested using the phantom data. As

stated above, this algorithm also calculates the scale as part of finding the rotational offset accurately so that is also shown in the results (see Table 1).

	Hi-SNR	Mid-SNR	Low-SNR
$\overline{\theta} \pm \sigma_\theta{}^o$	4.00 ± 0.133	3.94 ± 0.112	3.98 ± 0.139
$\overline{s} \pm \sigma_s$	0.949 ± 0.0022	0.950 ± 0.0009	0.951 ± 0.0016
$\overline{SNR_T} \pm \sigma(dB)$	17.67 ± 2.39	8.09 ± 1.33	4.81 ± 1.01
$\overline{SNR_C} \pm \sigma(dB)$	16.35 ± 1.93	6.93 ± 0.55	3.93 ± 0.27

Table 1. Average result for recovery of rotational and scale transformation between the simulated TIRF and LSCM data sets. σ denotes the standard deviation over the 5 results.

5.1.1. Translation and scale

The algorithm for completing registration, through calculation of translation and pixel scale was also tested with the phantom image data. The TIRF image was rotated 4^o clockwise to correct for the rotational offset on the TIRF data. The estimate for scale was given as 0.92 to mimic slight error in microscope resolution calibration.

Euclidean distance			
	Hi-SNR	Mid-SNR	Low-SNR
image 1	1	0	0
image 2	0	1	1
image 3	1	0	2
image 4	0	0	0
image 5	0	0	0

Table 2. The Euclidean distance from the known coordinates (20,20) of registration in pixels for each image for different noise levels.

The recovered scales are shown in Table 3.

Scale			
	Hi-SNR	Mid-SNR	Low-SNR
$\overline{s} \pm \sigma_s$	0.949 ± 0.0015	0.948 ± 0.0012	0.950 ± 0.0024

Table 3. Average scale recovered from Phantom images distorted with 3 levels of noise.

5.2. Real microscopy data

5.2.1. Rotation

The rotational offset algorithm was used on four different TIRF-LSCM image pairs. These images were of HeLa cells expressing clathrin-GFP (a vesicle coat protein) with various levels of noise (levels similar to those in *Low -& Mid -SNR* i.e. $\approx 4 - 8dB$ for the phantom data). As the true rotational offset between the measurement devices is not known the algorithms results were compared to results obtained manually which were calculated as follows: two points in each image were joined with a line(between features present in both), the difference in angle of each line with respect to the horizontal gave the angular offset. This was calculated for each image pair.

The results shown in Table 4 agree with the manually calculated result, falling within approximately one sixth of the standard deviation on its result. The standard deviation on the results for the real data is similar to (approximately half) that of the standard deviation of the results for the known rotation in the phantom validation.

5.2.2. Translation

The translation and scale algorithm was tested on the same set of four real pairs of image data. The TIRF images were rotated by the pre-registration rotational correction calculated above: 1.05^o. Registration was then performed using the *Translation and Scale* algorithm. To verify that the calculated alignment had in fact left images spatially coincident a difference in squares similarity measure was used: $s_{\Delta x,\Delta y} = \sum_{i,j} \left(I_1(i,j) - I_2(i-\Delta x, j-\Delta y)\right)^2$. The displacement that gives the smallest value of $s_{\Delta x,\Delta y}$ is considered as the position for best alignment. This was calculated for the aligned images ($(\Delta x, \Delta y) = (0,0)$) and then at every location over a local range of displacements ($\pm$ 20 pixels in both x and y). The results for three of the four real images were, $\Delta x = 0$ and $\Delta y = 0$, for the other $\Delta x = -1$ and $\Delta y = +1$. The accuracy of the scale parameter is more difficult to test as the ground truth for the real microscopy images is not known its calculation relies on the translation and scale parameters being calculated accurately. For this reason it was not tested.

Recovered Rotation		
	Manual	Algorithm
$\overline{\theta} \pm \sigma_\theta$	0.92 ± 0.656	1.05 ± 0.0435

Table 4. Average real images calculated manually. σ_θ is the standard deviation.

6. DISCUSSION

In this paper we have presented a method for co-registration of TIRF and LSCM image data sets along with a method for its validation. The algorithms have been shown to perform well on simulated images over a range of noise levels. The results using real image data sets agreed well with validation results suggesting that the algorithms are fit for their intended purpose. Integrating two imaging techniques on one microscope, spatially aligning the data, and following these with a good particle tracking algorithm should allow for greater yield of information about the vesicle dynamics throughout its intracellular journey. The phantom images generated using the mathematical image formation processes defined here, combined with the appropriate motion models, can also be used to validate tracking algorithms.

7. REFERENCES

[1] L. Liang, H. Shen, P. De Camilli, and J. Duncan, "Tracking clathrin coated pits with a multiple hypothesis based method," *Medical Image Computing and Computer-Assisted Intervention–MICCAI 2010*, pp. 315–322, 2010.

[2] A. Genovesio, T. Liedl, V. Emiliani, W.J. Parak, M. Coppey-Moisan, and J.C. Olivo-Marin, "Multiple particle tracking in 3-d+ t microscopy: Method and application to the tracking of endocytosed quantum dots," *Image Processing, IEEE Transactions on*, vol. 15, no. 5, pp. 1062–1070, 2006.

[3] J. Rappoport, "Focusing on clathrin-mediated endocytosis," *Biochem. J*, vol. 412, pp. 415–423, 2008.

[4] D. Axelrod, "Total internal reflection fluorescence microscopy in cell biology," *Traffic*, vol. 2, no. 11, pp. 764–774, 2001.

[5] William T. E. Pitkeathly, Natalie S. Poulter, Ela Claridge, and Joshua Z. Rappoport, "Auto-align - multi modality fluorescence microscopy image co-registration," *Traffic*, pp. no–no, 2011.

[6] JP Lewis, "Fast normalized cross-correlation," in *Vision Interface*, 1995, vol. 10, pp. 120–123.

[7] R.H. Webb, "Confocal optical microscopy," *Reports on Progress in Physics*, vol. 59, pp. 427, 1996.